Anomalous thermal broadening in the Shastry-Sutherland model and SrCu$_2$(BO$_3$)$_2$

Zhenjiu Wang,[1, 2, *] Paul McClarty,[2, 3, †] Dobromila Dankova,[2] Andreas Honecker,[4] and Alexander Wietek[2, ‡]

[1]*Arnold Sommerfeld Center for Theoretical Physics, University of Munich, Theresienstr. 37, 80333 Munich, Germany*
[2]*Max Planck Institute for the Physics of Complex Systems, Nöthnitzer Strasse 38, Dresden 01187, Germany*
[3]*Laboratoire Léon Brillouin, CEA, CNRS, Université Paris-Saclay, CEA Saclay, 91191 Gif-sur-Yvette, France*
[4]*Laboratoire de Physique Théorique et Modélisation, CNRS UMR 8089,*
CY Cergy Paris Université, 95302 Cergy-Pontoise, France
(Dated: May 28, 2024)

The quantum magnet SrCu$_2$(BO$_3$)$_2$ and its remarkably accurate theoretical description, the spin-1/2 Shastry-Sutherland model, host a variety of intriguing phenomena such as a dimer ground state with a nearly flat band of triplon excitations, a series of magnetization plateaux, and a possible pressure-induced deconfined quantum critical point. One open puzzle originating from inelastic neutron scattering and Raman experiments is the anomalous broadening of the triplon modes at relatively low temperatures compared to the triplon gap Δ. We demonstrate that the experimentally observed broadening is captured by the Shastry-Sutherland model. To this end, we develop a numerical simulation method based on matrix-product states to simulate dynamical spectral functions at nonzero temperatures accurately. Perturbative calculations identify the origin of this phenomenon as a small energy scale compared to Δ between single triplon and bound triplon states at the experimentally relevant model parameters.

Introduction One of the most exquisite examples of geometric frustration in quantum magnetism is the spin-1/2 Shastry-Sutherland model in which frustrated antiferromagnetic triangular units support an exact dimer covering in two dimensions over a significant range of exchange couplings [1]. Simple though the ground state in this model exemplifies nicely the effect of destructive interference on triangular units that is the heart of geometrical frustration the exploration of which has formed an entire field of research. Today studies of highly frustrated magnets range over rich and complex physics on kagome, pyrochlore, and other lattices [2]. There are however further pillars to the fame of the Shastry-Sutherland model. One is the discovery, many years after the original theory paper, of a material SrCu$_2$(BO$_3$)$_2$, that almost perfectly realizes the dimer phase of the model [3, 4]. This material, albeit one of thousands of magnetic materials, has consistently stood out for the surprises and puzzles that it has generated and continues to produce over twenty years after the first experiments [3–43]. These include the famous series of magnetization plateaux reaching up to around 100 T [3, 5–16], observations of nearly flat triplon excitations about the dimer phase [19, 21], IR, Raman and neutron studies exploring the triplons and the tower of bound state excitations [17–23], topological triplons coming from small exchange anisotropies [22, 27–29], experiments observing a plaquette phase in the material at high pressures and investigations of the nature of the phase transition to this phase [32, 34–40] including the tantalizing possibility of realizing deconfined criticality on the boundary between Néel order and the plaquette phase [41, 42]. The Shastry-Sutherland model frames all these experimental discoveries and both model and material have provided an important proving ground for new numerical and analytical tools. In fact, studies of SrCu$_2$(BO$_3$)$_2$ have turned out to be almost a microcosm for the development of quantum magnetism as a whole. For example, the low entanglement dimer phase was an attractive target for tensor network methods which now have captured much of the complexity of the magnetic field-induced phase diagram as crystals of condensed bound states [33]. Related techniques have captured also the thermodynamics of the model [43].

In this paper, we consider a further curiosity of SrCu$_2$(BO$_3$)$_2$ − a dramatic broadening of the triplon modes with increasing temperature uncovered by inelastic neutron scattering [19, 21, 44] and corroborated by Raman scattering [18, 23]. Thermal broadening of excitations is entirely to be expected in any correlated magnetic system. The peculiarity of SrCu$_2$(BO$_3$)$_2$ is its sensitivity to thermal excitations as well as the extent of the effect in the crossover to the paramagnetic state. To be concrete, the triplon excitations are gapped at about 3 meV or about 30 K, and significant broadening is observed by around 5 K, while the Bose factor at this temperature is about 3×10^{-3} so the triplons are undoubtedly very dilute. By 15 K the neutron intensity is broadened into a nearly featureless continuum. In the following, we show how to capture this effect quantitatively and provide insight into the microscopic mechanism that underlies it. On small cluster sizes up to $N = 20$ sites, a finite-temperature Lanczos study [45] reported anomalous thermal broadening but left results on larger system sizes desirable. In some sense, this work reflects the natural course of development in understanding low-dimensional magnetic systems using state-of-the-art numerical tools. Tensor network tools were first brought to bear on the ground states [16, 33, 46–48] then the thermodynamics [43, 49–52] and now it has become feasible to consider the nonzero temperature dynamics of extended two-dimensional frustrated quantum magnets.

The Shastry-Sutherland Model and its Experimental Realization The Shastry-Sutherland model is a localized spin-1/2 model formulated on the lattice illustrated in Fig. 1(a) [1]. The Hamiltonian is given by,

$$H = J_D \sum_{\langle i,j \rangle_D} \boldsymbol{S}_i \cdot \boldsymbol{S}_j + J \sum_{\langle\langle i,j \rangle\rangle} \boldsymbol{S}_i \cdot \boldsymbol{S}_j, \qquad (1)$$
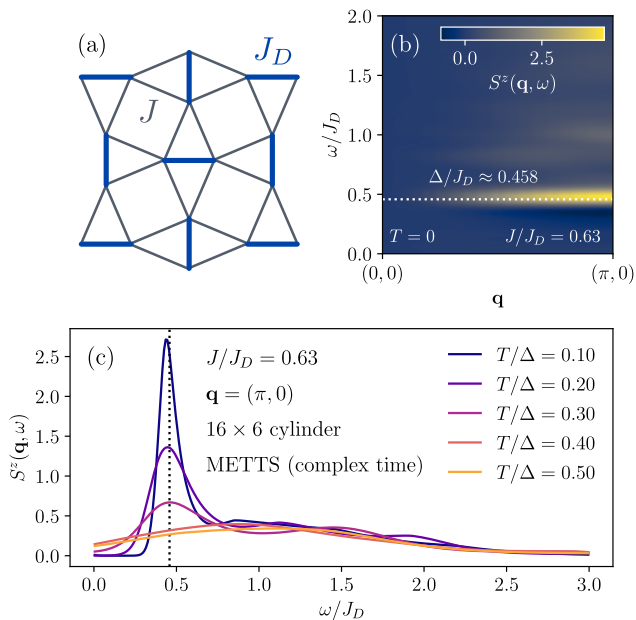
FIG. 1. (a) Geometry of the Shastry-Sutherland lattice. The intradimer couplings J_D are shown in blue and the interdimer couplings J in grey. (b) Dynamical spin structure factor $S(\boldsymbol{q}, \omega)$ at $T = 0$ from dynamical DMRG simulations on a 16×6 cylinder for a cut through the Brillouin zone from $(0,0)$ to $(\pi, 0)$ exhibiting a flat triplon band at energies around the triplet gap $\Delta \approx 0.458 J_D$. (c) $S((\pi, 0), \omega)$ for various temperatures from the proposed dynamical METTS simulations on a 16×6 cylinder, employing the analytical complex time algorithm as proposed in the companion paper [55]. The triplon peak at Δ melts into a broad continuum at temperatures that are a fraction of the triplon gap Δ.

where J_D denote the intradimer couplings and J the interdimer couplings. When $J = 0$ the ground state has isolated singlets living on the J_D bonds and canonical excitations are spin $S = 1$ triplets in the local dimers. When J is switched on each singlet couples via its two component spins to a single site on neighboring singlets. This geometrical frustration endows the singlets with stability such that the dimer covering survives as an exact eigenstate for all couplings and in the ground state up a $J/J_D \approx 0.67$ as determined numerically.

The lowest-lying excited states, for small J/J_D, are coupled triplet excitations called *triplons*. As the model and ground state are spin-rotationally symmetric, the triplons are three-fold degenerate. One might expect the coupled triplets to acquire some dispersion on the scale of J. However, it turns out that triplon hopping is suppressed by the magnetic frustration with the leading order contribution appearing to $O((J/J_D)^6)$ [7, 24, 26, 53, 54] − so the triplons are very nearly localized even close to the phase boundary out of the dimer phase resulting in a flat band of triplon excitations, cf. Fig. 1(b).

The material $SrCu_2(BO_3)_2$ with spin one-half copper ions realizes the Shastry-Sutherland model to a good approximation. At ambient pressure J/J_D has been experimentally esti-

mated to be 0.63 [7, 25, 43] so it lies at the edge of the dimer phase. Observations of the triplons reveal the bandwidth to be about one-tenth of the gap and therefore significantly larger than in the pure Shastry-Sutherland model. This indicates the presence of small anisotropies that are known to be predominantly Dzyaloshinskii-Moriya or antisymmetric exchange that we neglect here. Our results imply that these small corrections to the pristine Shastry-Sutherland model play a negligible role in the thermal broadening to which we now turn.

The sensitivity of the quantum states of $SrCu_2(BO_3)_2$ to finite temperatures was first observed from the washing out of magnetization plateaux at around 1 K [3]. Later the neutron scattering intensity of the single triplon modes was seen to fall off faster with increasing temperature than would be expected on the basis of the 35 K gap [19, 21, 44]. Indeed, the triplons are almost completely washed out by about 10 K leaving a broad continuum of intensity. This behavior is consistent with Raman measurements that are more sensitive to singlet intensity [18, 23]. It has been suspected for a long time that the unusual temperature dependence originates from the delicate nature of the frustration-induced dimer formation and, in particular, that only a very dilute concentration of thermal triplet states is sufficient to delocalize the dimers.

Thermal broadening from dynamical METTS We will now demonstrate the dynamics of the pure Shastry-Sutherland model to accurately capture the effect of the triplon thermal broadening in $SrCu_2(BO_3)_2$ with close agreement with experimental measurements. Our simulation is based on a numerical technique for evaluating dynamical spectral functions at nonzero temperature, based on the idea of minimally entangled typical thermal states [49, 50, 56, 57]. In the companion paper [55], we introduce this technique in detail and benchmark it against more traditional techniques where such a comparison is possible. The principal advantage of dynamical METTS is that it allows one to address significantly larger system sizes than previously possible. The method is performed in two distinct modes. With the real-time evolution algorithm, we directly simulate the dynamical correlation function,

$$\mathcal{C}_{AB}(t) = \langle A(t) B \rangle_\beta = \langle e^{iHt} A e^{-iHt} B \rangle_\beta, \qquad (2)$$

at nonzero temperature ($T = 1/\beta$) up to a final time Ω, after which a Fourier transform yields the desired spectral function. The dynamical correlation functions can be fully converged on $W = 4$ cylinders at all investigated temperatures for the Shastry-Sutherland model. Here, we chose a simulation time horizon of $\Omega/J_D = 50$.

This method yields highly accurate results for smaller cylinders, where even the temperature dependence of secondary and tertiary peaks can be resolved. However, since there are limitations in system size we introduce a complex-time evolution algorithm, where the dynamical correlation function is simulated on a contour in complex time coordinates and the spectral function is obtained via stochastic analytic continuation [58–61]. The fact that the correlation function is not just simulated on the imaginary-time axis yields
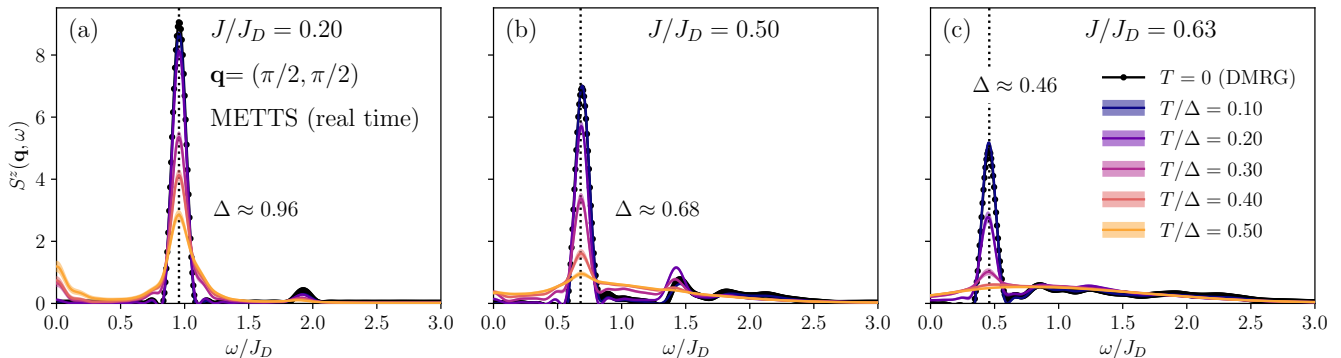
FIG. 2. Dynamical spin spectral functions evaluated at momentum $\boldsymbol{q} = (\pi/2, \pi/2)$ from dynamical METTS simulations on the 16×4 cylinder. Results at temperatures which are a fixed ratio of the triplet gap Δ as in Eq. (3) are shown. The triplet gap Δ is shown as the dashed line. (a) $J/J_D = 0.2$ (b) $J/J_D = 0.5$ (c) $J/J_D = 0.63$. Whereas the dominant peak close to the triplet gap is only weakly broadened for $J/J_D = 0.2$ it completely disappears at small fractions of the triplet gap for $J/J_D = 0.63$ in (c).

improvements in the ill-posedness of the analytical continuation. For all the necessary details, we refer to the companion paper [55].

Figure 2 shows the dynamical structure factor $S(\boldsymbol{q}, \omega)$ calculated for fixed $\boldsymbol{q} = (\pi/2, \pi/2)$ and for different temperatures and various J/J_D. For $J/J_D = 0.2$, the principal peak at $\omega/J_D = 0.96$ corresponds to the ground state to single triplon transition and there is a secondary peak at twice this energy coming mainly from the free two-triplon states. As the temperature increases the amplitude of both peaks decreases and both broaden and, at the same time, quasi-elastic intensity appears.

For larger values of J/J_D the single triplon peak comes down in energy and for a fixed temperature it is broader for larger values of J/J_D. Meanwhile, the two-triplon sector broadens into a continuum extending to both higher and lower energies. For $J/J_D = 0.63$ corresponding to the material the dynamical structure factor is a featureless continuum above around $T/\Delta = 0.4$ corresponding to about 14 K.

On the 16×6 cylinder we analogously observe the melting of the main triplon peak at temperatures $T/\Delta = 0.4$ in Fig. 1(c). There, results have been obtained using the complex-time evolution algorithm explained in the companion paper [55].

We now make a more direct comparison of the numerical results and the experiment. Figure 3 shows the cumulative spectral weight up to energy ω for different temperatures. The top panel is the numerical data at fixed momentum and the lower panel is the experimental data taken from Ref. [44]. The lower temperature data shows the single triplon peak as a rapid upturn in both numerics and experiment. At temperatures of about 0.4 of the triplet gap, the cumulative spectral weight increases almost linearly corresponding to an almost featureless continuum. This plot demonstrates that the numerical technique captures the thermal broadening in the material. In particular, the degree of broadening at a given temperature scale coincides between the simulation and the experiment.
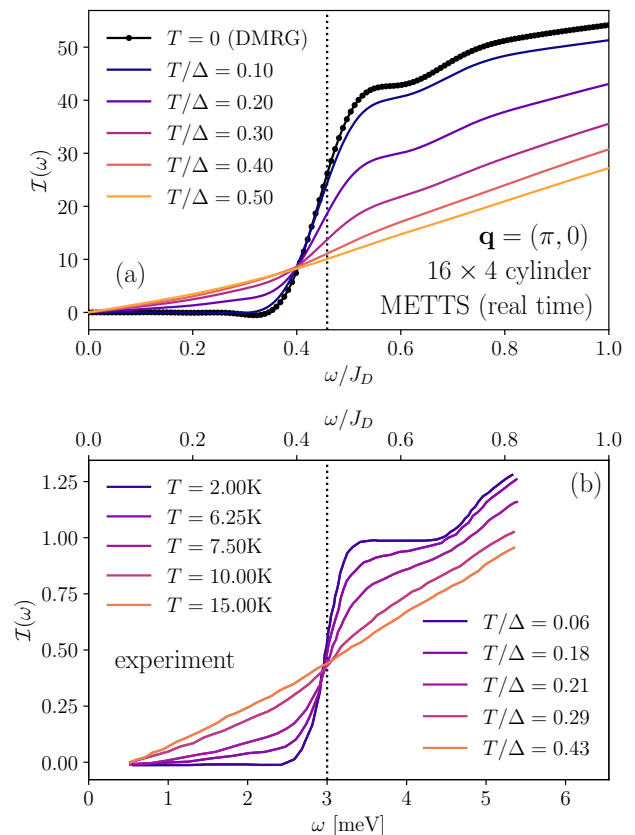

FIG. 3. Temperature dependence of the cumulative spectral weight as a function of energy. The lower panel is inelastic neutron scattering data (taken from Ref. [44]) on a powder sample. The data is momentum-integrated and resolved in energy. The data at five different temperatures reveals the progressive broadening of the central peak. The top panel is our numerical result for the cumulative spectral weight at momentum $(\pi, 0)$.

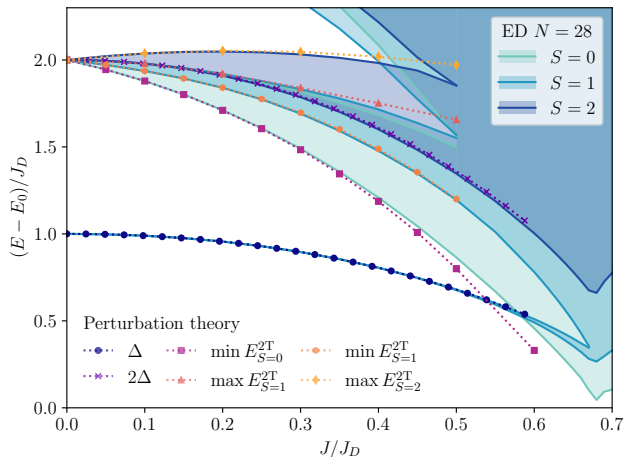Ref. [44] points out that the single triplon peak appears to

FIG. 4. Comparison of energy gaps between perturbation theory (PT) to third order in J/J_D and exact diagonalization (ED). The shaded regions show continua of spin-S states on a $N = 28$ cluster ($S = 0$ and 1 data adapted from Ref. [43]). The triplet gap Δ and the gap to the lowest $S = 0$ excitations agree well between PT and ED. At $J/J_D \gtrsim 0.6$ the lowest excited states are bound states of two triplons with $S = 0$, invisible in the spin structure factor but thermally activated prior to the triplon excitations for the experimentally relevant parameters $J/J_D = 0.63$.

FIG. 5. Dynamical structure factor at $J/J_D = 0.5$ and $\boldsymbol{q} = (2\pi, 0)$ computed from the low-temperature expansion described in the main text and supp. mat. [62]. The inset shows the evolution of the peak height with increasing temperature.

have one sharp component whose amplitude decreases with temperature and a broad temperature-dependent component, which is consistent with our numerics.

A few comments and caveats are necessary at this point. One is that the zero temperature peak is a delta function in principle. This is not realized in the numerics because of the inevitable finite time cutoff in the dynamics. The experimental single triplon peak also has a width at very low temperatures owing to instrumental resolution. Secondly, one plausible lesson to be drawn from the excellent agreement between theory and experiment is that the relevant physics is rather local. As we shall argue this originates from the almost perfect localization of the single triplon modes combined with the fact that small system sizes already capture the broad spectrum of bound-state modes as the relevant states have a short length scale. Finally, one might be concerned that the material has couplings beyond the Heisenberg model and that these may contribute to the thermal broadening. The good agreement between the numerical results and experiment is nevertheless suggestive that the pure Shastry-Sutherland model is largely responsible for the physics. We argue below that indeed the relevant scales are those coming from the Heisenberg model.

Physics of thermal broadening − Having seen that the Shastry-Sutherland model in a non-perturbative analysis leads to thermal broadening similar to that seen in $SrCu_2(BO_3)_2$ we now discuss the microscopic origin of this phenomenon.

To set the scene we briefly review some pertinent features of the model. As noted above, interactions mediated by the exchange J lead to a triplon dispersion, to leading order, only at the sixth order in the coupling [7, 24, 30] so, for the pa-
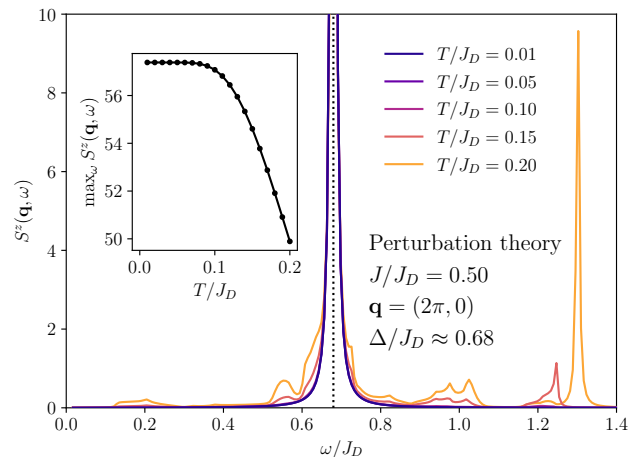
rameters corresponding to the material, the triplon modes are expected to be nearly flat. The flatness of the single particle modes further implies that the two-triplon continuum is very narrow in energy. The interactions, however, do have a significant effect on the triplon energy which is renormalized downwards as

$$\Delta = J_D \left[1 - (J/J_D)^2 - \frac{1}{2}(J/J_D)^3 - \frac{1}{8}(J/J_D)^4 \right] \quad (3)$$

to 4th order in perturbation theory [7, 24].

Complex collective physics in this model originates from the formation of bound states of triplons. The lowest-lying of these are bound states of two triplons which occur in the $S = 0, 1$, and 2 sectors of which the former contain those of lowest energy. Splitting of the different angular momentum sectors grows like $O(J)$ and the bandwidth in each sector like $O(J^2)$ so the localizing effects of frustration on single triplons are absent in the two-triplon sector. This disparity between the single and two-particle states sets this model apart from typical frustrated magnets. The gap between the single triplons and the lowest bound state excitations closes in the vicinity of $J/J_D = 0.6$. Remarkably real-space perturbation theory to third order in J/J_D leads to bound states with a bandwidth in good agreement with exact diagonalization. This is illustrated in Fig. 4 which reveals that the value of J/J_D at which the single and two-particle levels cross is slightly underestimated in the perturbation theory [62].

At zero temperature, the dynamical structure factor has been computed perturbatively in Ref. [31] and has a delta function peak at the single triplon energy at least when there is a separation of energies between the one and two-triplon states. At finite temperatures, one may formulate the problem

as a calculation of self-energy $\Sigma(\boldsymbol{q},\omega)$ to obtain susceptibility

$$\chi^{zz}(\boldsymbol{q},\omega) = \frac{D(\boldsymbol{q},\omega)}{1 - D(\boldsymbol{q},\omega)\Sigma(\boldsymbol{q},\omega)}, \qquad (4)$$

where D is the single triplon propagator and the zz component of the dynamical structure factor is chosen without losing generality. From this, we get the dynamic structure factor

$$S^{zz}(\boldsymbol{q},\omega) = -\frac{1}{\pi}\frac{1}{1 - e^{-\beta\omega}}\mathrm{Im}\left[\chi^{zz}(\boldsymbol{q},\omega)\right]. \qquad (5)$$

We compute the self-energy within a low-temperature expansion by matching the leading order appearance of the self-energy from Eq. (4) with those terms from the spectral representation of the dynamical correlator [62–64]

$$\langle S_i^z(\tau) S_j^z(0)\rangle = \frac{1}{Z}\sum_{m,n} e^{-\beta E_m}\langle m|S_i^z(\tau)|n\rangle\langle n|S_j^z(0)|m\rangle \qquad (6)$$

that contribute at low temperatures. This ends up meaning that we compute a re-summed self-energy of the form

$$\begin{aligned}&\Sigma(\boldsymbol{q},\omega)\\&= D^{-2}\left(C_{11} + C_{12} + C_{21} - e^{-\beta\epsilon}D - Z_1(1 - e^{-\beta\epsilon})D\right)\end{aligned} \qquad (7)$$

where C_{mn} are defined through $\chi^{zz}(\boldsymbol{q},\omega) = (1/Z)\sum_{mn} C_{mn}$ where the terms in the sum refer to m/n-triplon states and Z_1 is the single triplon contribution to the partition sum. The contribution C_{11} vanishes when working consistently to third order in J/J_{D} as the single triplons are dispersionless. The C_{12} and C_{21} contributions are split into pieces that come from free two-triplon states and from the bound states. The former contains a part that scales with the number of unit cells, N, which cancels with $Z_1(1 - e^{-\beta\epsilon})D$. The central contribution to the broad response in energy comes from the bound states.

Fig. 5 shows the resulting dynamical structure factor for $J/J_D = 0.5$ and for $\boldsymbol{q} = (2\pi, 0)$ where the single triplon intensity is maximal. Several temperatures are plotted between $T/J_D = 0.01$ up to 0.2 ($T/\Delta \approx 0.3$). Notably, the delta peak corresponding to the single triplon mode remains but its amplitude decreases with increasing temperature as shown in the inset. In addition to the single triplon peak, there is a broad response originating from the bound states that, as we have mentioned, have a bandwidth of the order of J. This broad component to the dynamical structure factor is bounded, for $J/J_D = 0.5$, by the gap between the triplon mode and the lowermost and uppermost bound state modes − namely $\Delta/J_D = 0.12$ and about 1.5.

To summarize, the perturbation theory gives an account of the broad inelastic response appearing at energies much smaller than the single triplon gap. Central to this is the "fine-tuning" in $SrCu_2(BO_3)_2$ such that it lies close to a phase boundary and the bound states have anomalously low energy. In "typical" gapped quantum magnets, two-particle states would arise at around 2Δ resulting in an inelastic response from energy Δ. In contrast, in "typical" gapless quantum magnets, a continuum of states and broadening are both to be expected at *zero* temperature so that effects of finite temperature will tend to be quantitative, not qualitative. In this way, we can understand why thermal broadening $SrCu_2(BO_3)_2$ stands out among quantum magnets.

Conclusion We investigated the origin of the anomalous thermal broadening observed in neutron scattering experiments of $SrCu_2(BO_3)_2$. By introducing a matrix-product state-based technique based on minimally entangled typical thermal states we demonstrated that this effect is accurately captured by the Shastry-Sutherland model on cylinders up to width $W = 6$. Moreover, we provide an intuitive explanation where bound states of two triplons proliferate below the single triplon gap at the experimentally relevant model parameters $J/J_D = 0.63$. By demonstrating the feasibility of studying finite-temperature dynamics using tensor network methods, this work paves the way for future investigations of frustrated quantum magnets at non-zero temperatures.

---

[*] zhenjiu.wang@physik.uni-muenchen.de
[†] Z. Wang and P. McClarty contributed equally to the manuscript.
[‡] awietek@pks.mpg.de

[1] B. Sriram Shastry and B. Sutherland, Exact ground state of a quantum mechanical antiferromagnet, Physica B+C **108**, 1069 (1981).

[2] C. Lacroix, P. Mendels, and F. Mila, *Introduction to frustrated magnetism: materials, experiments, theory*, Vol. 164 (Springer Science & Business Media, 2011).

[3] H. Kageyama, K. Yoshimura, R. Stern, N. V. Mushnikov, K. Onizuka, M. Kato, K. Kosuge, C. P. Slichter, T. Goto, and Y. Ueda, Exact Dimer Ground State and Quantized Magnetization Plateaus in the Two-Dimensional Spin System $SrCu_2(BO_3)_2$, Phys. Rev. Lett. **82**, 3168 (1999).

[4] H. Kageyama, K. Onizuka, T. Yamauchi, Y. Ueda, S. Hane, H. Mitamura, T. Goto, K. Yoshimura, and K. Kosuge, Anomalous Magnetizations in Single Crystalline $SrCu_2(BO_3)_2$, J. Phys. Soc. Jpn. **68**, 1821 (1999).

[5] K. Onizuka, H. Kageyama, Y. Narumi, K. Kindo, Y. Ueda, and T. Goto, 1/3 Magnetization Plateau in $SrCu_2(BO_3)_2$ - Stripe Order of Excited Triplets -, J. Phys. Soc. Jpn. **69**, 1016 (2000).

[6] K. Kodama, M. Takigawa, M. Horvatić, C. Berthier, H. Kageyama, Y. Ueda, S. Miyahara, F. Becca, and F. Mila, Magnetic Superstructure in the Two-Dimensional Quantum Antiferromagnet $SrCu_2(BO_3)_2$, Science **298**, 395 (2002).

[7] S. Miyahara and K. Ueda, Theory of the orthogonal dimer Heisenberg spin model for $SrCu_2(BO_3)_2$, J. Phys.: Condens.

Matter **15**, R327 (2003).

[8] M. Takigawa, K. Kodama, M. Horvatić, C. Berthier, H. Kageyama, Y. Ueda, S. Miyahara, F. Becca, and F. Mila, The $\frac{1}{8}$-magnetization plateau state in the 2D quantum antiferromagnet $SrCu_2(BO_3)_2$: spin superstructure, phase transition, and spin dynamics studied by high-field NMR, Physica B **346**, 27 (2004).

[9] K. Kodama, S. Miyahara, M. Takigawa, M. Horvatić, C. Berthier, F. Mila, H. Kageyama, and Y. Ueda, Field-induced effects of anisotropic magnetic interactions in $SrCu_2(BO_3)_2$, J. Phys.: Condens. Matter **17**, L61 (2005).

[10] F. Levy, I. Sheikin, C. Berthier, M. Horvatić, M. Takigawa, H. Kageyama, T. Waki, and Y. Ueda, Field dependence of the quantum ground state in the Shastry-Sutherland system $SrCu_2(BO_3)_2$, Europhys. Lett. **81**, 67004 (2008).

[11] S. E. Sebastian, N. Harrison, P. Sengupta, C. D. Batista, S. Francoual, E. Palm, T. Murphy, N. Marcano, H. A. Dabkowska, and B. D. Gaulin, Fractalization drives crystalline states in a frustrated spin system, Proc. Natl. Acad. Sci. USA **105**, 20157 (2008).

[12] M. Jaime, R. Daou, S. A. Crooker, F. Weickert, A. Uchida, A. E. Feiguin, C. D. Batista, H. A. Dabkowska, and B. D. Gaulin, Magnetostriction and magnetic texture to 100.75 Tesla in frustrated $SrCu_2(BO_3)_2$, Proc. Natl. Acad. Sci. USA **109**, 12404 (2012).

[13] M. Takigawa, M. Horvatić, T. Waki, S. Krämer, C. Berthier, F. Lévy-Bertrand, I. Sheikin, H. Kageyama, Y. Ueda, and F. Mila, Incomplete Devil's Staircase in the Magnetization Curve of $SrCu_2(BO_3)_2$, Phys. Rev. Lett. **110**, 067210 (2013).

[14] Y. H. Matsuda, N. Abe, S. Takeyama, H. Kageyama, P. Corboz, A. Honecker, S. R. Manmana, G. R. Foltin, K. P. Schmidt, and F. Mila, Magnetization of $SrCu_2(BO_3)_2$ in Ultrahigh Magnetic Fields up to 118 T, Phys. Rev. Lett. **111**, 137204 (2013).

[15] S. Haravifard, D. Graf, A. E. Feiguin, C. D. Batista, J. C. Lang, D. M. Silevitch, G. Srajer, B. D. Gaulin, H. A. Dabkowska, and T. F. Rosenbaum, Crystallization of spin superlattices with pressure and field in the layered magnet $SrCu_2(BO_3)_2$, Nat. Commun. **7**, 11956 (2016).

[16] T. Nomura, P. Corboz, A. Miyata, S. Zherlitsyn, Y. Ishii, Y. Kohama, Y. H. Matsuda, A. Ikeda, C. Zhong, H. Kageyama, and F. Mila, Unveiling new quantum phases in the Shastry-Sutherland compound $SrCu_2(BO_3)_2$ up to the saturation magnetic field, Nat. Commun. **14**, 3769 (2023).

[17] H. Nojiri, H. Kageyama, K. Onizuka, Y. Ueda, and M. Motokawa, Direct Observation of the Multiple Spin Gap Excitations in Two-Dimensional Dimer System $SrCu_2(BO_3)_2$, J. Phys. Soc. Jpn. **68**, 2906 (1999).

[18] P. Lemmens, M. Grove, M. Fischer, G. Güntherodt, V. N. Kotov, H. Kageyama, K. Onizuka, and Y. Ueda, Collective Singlet Excitations and Evolution of Raman Spectral Weights in the 2D Spin Dimer Compound $SrCu_2(BO_3)_2$, Phys. Rev. Lett. **85**, 2605 (2000).

[19] H. Kageyama, M. Nishi, N. Aso, K. Onizuka, T. Yosihama, K. Nukui, K. Kodama, K. Kakurai, and Y. Ueda, Direct evidence for the localized single-triplet excitations and the dispersive multitriplet excitations in $SrCu_2(BO_3)_2$, Phys. Rev. Lett. **84**, 5876 (2000).

[20] T. Rõõm, U. Nagel, E. Lippmaa, H. Kageyama, K. Onizuka, and Y. Ueda, Far-infrared study of the two-dimensional dimer spin system $SrCu_2(BO_3)_2$, Phys. Rev. B **61**, 14342 (2000).

[21] B. D. Gaulin, S. H. Lee, S. Haravifard, J. P. Castellan, A. J. Berlinsky, H. A. Dabkowska, Y. Qiu, and J. R. D. Copley, High-Resolution Study of Spin Excitations in the Singlet Ground State of $SrCu_2(BO_3)_2$, Phys. Rev. Lett. **93**, 267202 (2004).

[22] P. A. McClarty, F. Krüger, T. Guidi, S. F. Parker, K. Refson, A. W. Parker, D. Prabhakaran, and R. Coldea, Topological triplon modes and bound states in a Shastry–Sutherland magnet, Nat. Phys. **13**, 736 (2017).

[23] D. Wulferding, Y. Choi, S. Lee, M. A. Prosnikov, Y. Gallais, P. Lemmens, C. Zhong, H. Kageyama, and K.-Y. Choi, Thermally populated versus field-induced triplon bound states in the Shastry-Sutherland lattice $SrCu_2(BO_3)_2$, npj Quantum Materials **6**, 102 (2021).

[24] S. Miyahara and K. Ueda, Exact Dimer Ground State of the Two Dimensional Heisenberg Spin System $SrCu_2(BO_3)_2$, Phys. Rev. Lett. **82**, 3701 (1999).

[25] S. Miyahara and K. Ueda, Thermodynamic properties of three-dimensional orthogonal dimer model for $SrCu_2(B0_3)_2$, J. Phys. Soc. Jpn. Suppl B **69**, 72.

[26] C. Knetter, A. Bühler, E. Müller-Hartmann, and G. S. Uhrig, Dispersion and Symmetry of Bound States in the Shastry-Sutherland Model, Phys. Rev. Lett. **85**, 3958 (2000).

[27] O. Cépas, K. Kakurai, L. P. Regnault, T. Ziman, J. P. Boucher, N. Aso, M. Nishi, H. Kageyama, and Y. Ueda, Dzyaloshinski-Moriya Interaction in the 2D Spin Gap System $SrCu_2(BO_3)_2$, Phys. Rev. Lett. **87**, 167205 (2001).

[28] J. Romhányi, K. Totsuka, and K. Penc, Effect of Dzyaloshinskii-Moriya interactions on the phase diagram and magnetic excitations of $SrCu_2(BO_3)_2$, Phys. Rev. B **83**, 024413 (2011).

[29] J. Romhányi, K. Penc, and R. Ganesh, Hall effect of triplons in a dimerized quantum magnet, Nat. Commun. **6**, 6805 (2015).

[30] K. Totsuka, S. Miyahara, and K. Ueda, Low-Lying Magnetic Excitation of the Shastry-Sutherland Model, Phys. Rev. Lett. **86**, 520 (2001).

[31] C. Knetter and G. S. Uhrig, Dynamic structure factor of the two-dimensional Shastry-Sutherland model, Phys. Rev. Lett. **92**, 027204 (2004).

[32] T. Waki, K. Arai, M. Takigawa, Y. Saiga, Y. Uwatoko, H. Kageyama, and Y. Ueda, A Novel Ordered Phase in $SrCu_2(BO_3)_2$ under High Pressure, J. Phys. Soc. Jpn. **76**, 073710 (2007).

[33] P. Corboz and F. Mila, Crystals of Bound States in the Magnetization Plateaus of the Shastry-Sutherland Model, Phys. Rev. Lett. **112**, 147203 (2014).

[34] M. E. Zayed, C. Rüegg, J. L. J., A. M. Läuchli, C. Panagopoulos, S. S. Saxena, M. Ellerby, D. F. McMorrow, T. Strässle, S. Klotz, G. Hamel, R. A. Sadykov, V. Pomjakushin, M. Boehm, M. Jiménez–Ruiz, A. Schneidewind, E. Pomjakushina, M. Stingaciu, K. Conder, and H. M. Rønnow, 4-spin plaquette singlet state in the Shastry–Sutherland compound $SrCu_2(BO_3)_2$, Nat. Phys. **13**, 962 (2017).

[35] S. Haravifard, A. Banerjee, J. C. Lang, G. Srajer, D. M. Silevitch, B. D. Gaulin, H. A. Dabkowska, and T. F. Rosenbaum, Continuous and discontinuous quantum phase transitions in a model two-dimensional magnet, Proc. Natl. Acad. Sci. USA **109**, 2286 (2012).

[36] T. Sakurai, Y. Hirao, K. Hijii, S. Okubo, H. Ohta, Y. Uwatoko, K. Kudo, and Y. Koike, Direct Observation of the Quantum Phase Transition of $SrCu_2(BO_3)_2$ by High-Pressure and Terahertz Electron Spin Resonance, J. Phys. Soc. Jpn. **87**, 033701 (2018).

[37] C. Boos, S. P. G. Crone, I. A. Niesen, P. Corboz, K. P. Schmidt, and F. Mila, Competition between intermediate plaquette phases in $SrCu_2(BO_3)_2$ under pressure, Phys. Rev. B **100**, 140413 (2019).

[38] D. I. Badrtdinov, A. A. Tsirlin, V. V. Mazurenko, and F. Mila, $SrCu_2(BO_3)_2$ under pressure: A first-principles study, Phys.

Rev. B **101**, 224424 (2020).

[39] J. L. Jiménez, S. P. G. Crone, E. Fogh, M. E. Zayed, R. Lortz, E. Pomjakushina, K. Conder, A. M. Läuchli, L. Weber, S. Wessel, A. Honecker, B. Normand, C. Rüegg, P. Corboz, H. M. Rønnow, and F. Mila, A quantum magnetic analogue to the critical point of water, Nature **592**, 370 (2021).

[40] P. C. G. Vlaar and P. Corboz, Tensor network study of the Shastry-Sutherland model with weak interlayer coupling, SciPost Phys. **15**, 126 (2023).

[41] J. Yang, A. W. Sandvik, and L. Wang, Quantum criticality and spin liquid phase in the Shastry-Sutherland model, Phys. Rev. B **105**, L060409 (2022).

[42] J. Y. Lee, Y.-Z. You, S. Sachdev, and A. Vishwanath, Signatures of a Deconfined Phase Transition on the Shastry-Sutherland Lattice: Applications to Quantum Critical SrCu$_2$(BO$_3$)$_2$, Phys. Rev. X **9**, 041037 (2019).

[43] A. Wietek, P. Corboz, S. Wessel, B. Normand, F. Mila, and A. Honecker, Thermodynamic properties of the Shastry-Sutherland model throughout the dimer-product phase, Phys. Rev. Res. **1**, 033038 (2019).

[44] M. E. Zayed, C. Rüegg, T. Strässle, U. Stuhr, B. Roessli, M. Ay, J. Mesot, P. Link, E. Pomjakushina, M. Stingaciu, K. Conder, and H. M. Rønnow, Correlated Decay of Triplet Excitations in the Shastry-Sutherland Compound SrCu$_2$(BO$_3$)$_2$, Phys. Rev. Lett. **113**, 067201 (2014).

[45] S. El Shawish, J. Bonča, and I. Sega, Dynamic spin structure factor of SrCu$_2$(BO$_3$)$_2$ at finite temperatures, Phys. Rev. B **72**, 184409 (2005).

[46] P. Corboz and F. Mila, Tensor network study of the Shastry-Sutherland model in zero magnetic field, Phys. Rev. B **87**, 115144 (2013).

[47] P. Czarnik, M. M. Rams, P. Corboz, and J. Dziarmaga, Tensor network study of the $m = \frac{1}{2}$ magnetization plateau in the Shastry-Sutherland model at finite temperature, Phys. Rev. B **103**, 075113 (2021).

[48] P. C. G. Vlaar and P. Corboz, Tensor network study of the Shastry-Sutherland model with weak interlayer coupling, SciPost Phys. **15**, 126 (2023).

[49] A. Wietek, Y.-Y. He, S. R. White, A. Georges, and E. M. Stoudenmire, Stripes, antiferromagnetism, and the pseudogap in the doped Hubbard model at finite temperature, Phys. Rev. X **11**, 031007 (2021).

[50] A. Wietek, R. Rossi, F. Šimkovic, M. Klett, P. Hansmann, M. Ferrero, E. M. Stoudenmire, T. Schäfer, and A. Georges, Mott insulating states with competing orders in the triangular lattice Hubbard model, Phys. Rev. X **11**, 041013 (2021).

[51] C. Feng, A. Wietek, E. M. Stoudenmire, and R. R. P. Singh, Order, disorder, and monopole confinement in the spin-$\frac{1}{2}$ XXZ model on a pyrochlore tube, Phys. Rev. B **106**, 075135 (2022).

[52] C. Feng, E. M. Stoudenmire, and A. Wietek, Bose-Einstein condensation in honeycomb dimer magnets and Yb$_2$Si$_2$O$_7$, Phys. Rev. B **107**, 205150 (2023).

[53] Z. Weihong, C. J. Hamer, and J. Oitmaa, Series expansions for a Heisenberg antiferromagnetic model for SrCu$_2$(BO)$_3$)$_2$, Phys. Rev. B **60**, 6608 (1999).

[54] C. Knetter, E. Müller-Hartmann, G. S. Uhrig, and E. Müller-Hartmann, Symmetries and triplet dispersion in a modified Shastry-Sutherland model for SrCu$_2$(BO$_3$)$_2$, J. Phys.: Condens. Matter **12**, 9069 (2000).

[55] Z. Wang, P. McClarty, D. Dankova, A. Honecker, and A. Wietek, Spectroscopy and complex-time correlations using minimally entangled typical thermal states, to appear (2024).

[56] S. R. White, Minimally Entangled Typical Quantum States at Finite Temperature, Phys. Rev. Lett. **102**, 190601 (2009).

[57] E. M. Stoudenmire and S. R. White, Minimally entangled typical thermal state algorithms, New J. Phys. **12**, 055026 (2010).

[58] R. N. Silver, D. S. Sivia, and J. E. Gubernatis, Maximum-entropy method for analytic continuation of quantum Monte Carlo data, Phys. Rev. B **41**, 2380 (1990).

[59] A. W. Sandvik, Stochastic method for analytic continuation of quantum Monte Carlo data, Phys. Rev. B **57**, 10287 (1998).

[60] K. S. D. Beach, Identifying the maximum entropy method as a special limit of stochastic analytic continuation (2004), arXiv:cond-mat/0403055 [cond-mat.str-el].

[61] H. Shao and A. W. Sandvik, Progress on stochastic analytic continuation of quantum Monte Carlo data, Phys. Rep. **1003**, 1 (2023).

[62] See Supplemental Material for details on the perturbation theory, including Refs. [65–69].

[63] F. H. L. Essler and R. M. Konik, Finite-temperature lineshapes in gapped quantum spin chains, Phys. Rev. B **78**, 100403 (2008).

[64] A. J. A. James, F. H. L. Essler, and R. M. Konik, Finite-temperature dynamical structure factor of alternating Heisenberg chains, Phys. Rev. B **78**, 094411 (2008).

[65] E. S. Klyushina, A. C. Tiegel, B. Fauseweh, A. T. M. N. Islam, J. T. Park, B. Klemke, A. Honecker, G. S. Uhrig, S. R. Manmana, and B. Lake, Magnetic excitations in the $S = \frac{1}{2}$ antiferromagnetic-ferromagnetic chain compound BaCu$_2$V$_2$O$_8$ at zero and finite temperature, Phys. Rev. B **93**, 241109 (2016).

[66] B. Fauseweh, F. Groitl, T. Keller, K. Rolfs, D. A. Tennant, K. Habicht, and G. S. Uhrig, Time-dependent correlations in quantum magnets at finite temperature, Phys. Rev. B **94**, 180404 (2016).

[67] S. Sachdev and R. N. Bhatt, Bond-operator representation of quantum spins: Mean-field theory of frustrated quantum Heisenberg antiferromagnets, Phys. Rev. B **41**, 9323 (1990).

[68] T. Momoi and K. Totsuka, Magnetization plateaus as insulator-superfluid transitions in quantum spin systems, Phys. Rev. B **61**, 3231 (2000).

[69] T. Momoi and K. Totsuka, Magnetization plateaus of the Shastry-Sutherland model for SrCu$_2$(BO$_3$)$_2$: Spin-density wave, supersolid, and bound states, Phys. Rev. B **62**, 15067 (2000).

Supplementary Material for "Anomalous thermal broadening in the Shastry-Sutherland model and $SrCu_2(BO_3)_2$"

(Dated: May 28, 2024)

Abstract

In this supplementary section, we provide details of the thermal broadening calculation from perturbation theory.

CONTENTS

THERMAL BROADENING CALCULATION OUTLINE

In this supplementary section we carry out a calculation of the dynamical structure factor for the Shastry-Sutherland model

$$S^{\alpha\beta}(\boldsymbol{q},\omega) = -\frac{1}{\pi}\frac{1}{1-e^{-\beta\omega}}\mathrm{Im}\left[\chi^{\alpha\beta}(\boldsymbol{q},\omega)\right], \tag{1}$$

where $\chi^{\alpha\beta}(\boldsymbol{q},\omega)$ is the momentum and energy dependent susceptibility and α,β are spin components. As the model is isotropic in spin space, without loss of generality we compute the zz component. This is given by

$$\chi^{zz}(\boldsymbol{q},\omega) = -\int_0^\beta d\tau e^{i\omega_n\tau}\frac{1}{4N}\sum_{\boldsymbol{I},\boldsymbol{J}}e^{-i\boldsymbol{q}\cdot(\boldsymbol{I}-\boldsymbol{J})}\left.\langle S_{\boldsymbol{I}}^z(\tau)S_{\boldsymbol{J}}^z(0)\rangle\right|_{\omega_n\to\eta-i\omega}. \tag{2}$$

Here N is the number of primitive lattice cells and the sum runs over all spins indexed by primitive cell, dimer $\boldsymbol{d}$ and spin $\boldsymbol{s}$ e.g. $\boldsymbol{I} = \boldsymbol{R}_I + \boldsymbol{d} + \boldsymbol{s}(\boldsymbol{d})$.

The correlator $C(\boldsymbol{x} \equiv \boldsymbol{I} - \boldsymbol{J}, \tau) \equiv \langle S_{\boldsymbol{I}}^z(\tau) S_{\boldsymbol{J}}^z(0) \rangle$ can be written as

$$C(\boldsymbol{x}, \tau) = \frac{1}{Z} \sum_{m,n} e^{-\beta E_m} \langle m | S_{\boldsymbol{I}}^z(\tau) | n \rangle \langle n | S_{\boldsymbol{J}}^z(0) | m \rangle, \tag{3}$$

where states labeled by m and n run over the exact eigenstates of the system.

We then separate the states into sets Γ_r, Γ_s defined by the triplon number r, s. Using

$$\langle \Gamma_r | S_{\boldsymbol{I}}^z(\tau) | \Gamma_s \rangle = e^{-\tau(E_{\Gamma_s} - E_{\Gamma_r})} \langle \Gamma_r | S_{\boldsymbol{I}}^z | \Gamma_s \rangle \tag{4}$$

and carrying out the imaginary time integration we find:

$$\chi^{zz}(\boldsymbol{q}, \omega) = \frac{1}{4N} \frac{1}{Z} \sum_{\Gamma_r, \Gamma_s} \sum_{\boldsymbol{I}, \boldsymbol{J}} e^{-i\boldsymbol{q}\cdot(\boldsymbol{I}-\boldsymbol{J})} \langle \Gamma_r | S_{\boldsymbol{I}}^z | \Gamma_s \rangle \langle \Gamma_s | S_{\boldsymbol{J}}^z | \Gamma_r \rangle \left(\frac{e^{-\beta E_{\Gamma_r}} - e^{-\beta E_{\Gamma_s}}}{\omega + i\eta + E_{\Gamma_r} - E_{\Gamma_s}} \right). \tag{5}$$

The strategy we adopt for computing the thermal broadening of the dynamical structure factor originates from Refs. [1, 2] which contain calculations of thermal broadening in spin chains and, in particular, a demonstration of asymmetric lineshape broadening in the models considered (alternative variants exist, see, e.g., Refs. [3, 4]). The first simplification we make is to focus on temperatures smaller than the single triplon gap Δ. Since higher energy excitations are suppressed by the Boltzmann weight we concentrate only on contributions to the susceptibility coming from few triplon excitations. In particular, we write

$$\chi^{zz}(\boldsymbol{q}, \omega) = \frac{1}{Z} \sum_{r,s=0}^{\infty} C_{rs} \approx \frac{1}{Z} \left(C_{10} + C_{01} + C_{11} + C_{12} + C_{21} \right) \tag{6}$$

where the sum is over all r, s triplon contributions.

We use notation $D(\boldsymbol{q}, \omega)$ for the single triplon propagator which is simply

$$(1 - e^{-\beta\Delta}) D(\boldsymbol{q}, \omega) = C_{10} + C_{01} \tag{7}$$

with

$$D(\boldsymbol{q}, \omega) = \frac{1}{8} \left[2 - \cos\left(\frac{q_x + q_y}{2} \right) - \cos\left(\frac{q_x - q_y}{2} \right) \right] \left(\frac{1}{\omega + i\eta - \Delta} - \frac{1}{\omega + i\eta + \Delta} \right). \tag{8}$$

Now we suppose that interactions between the triplons are folded into a self-energy $\Sigma(\boldsymbol{q}, \omega)$ appearing in a Dyson expansion for the susceptibility component

$$\chi^{zz}(\boldsymbol{q}, \omega) = \frac{D(\boldsymbol{q}, \omega)}{1 - D(\boldsymbol{q}, \omega) \Sigma(\boldsymbol{q}, \omega)} \approx D(\boldsymbol{q}, \omega) \left(1 + D(\boldsymbol{q}, \omega) \Sigma(\boldsymbol{q}, \omega) \right). \tag{9}$$

3

Matching Eqs. (6) and (9) leads to a resummed expression for the self-energy

$$\Sigma(\boldsymbol{q}, \omega) = D^{-2}\left(C_{11} + C_{12} + C_{21} - e^{-\beta\epsilon}D - Z_1(1 - e^{-\beta\epsilon})D\right) \tag{10}$$

where the partition sum has been split into contributions labeled by triplon number $Z = 1 + Z_1 + Z_2 + \ldots$ and where we have neglected Z_2 and higher terms as they are suppressed exponentially at low temperatures.

BOND WAVE THEORY AND LATTICE CONVENTIONS

The Shastry-Sutherland model is a spin one-half localized spin model on a two dimensional lattice with a square primitive cell $\boldsymbol{R}_1 = (1,0)$ and $\boldsymbol{R}_2 = (0,1)$, $\boldsymbol{R}_I = m_I \boldsymbol{R}_1 + n_I \boldsymbol{R}_2$, and a four sublattice basis:

$$\boldsymbol{r}_{A1} = (0,0)\,, \quad \boldsymbol{r}_{A2} = \left(\frac{1}{2}, \frac{1}{2}\right)\,, \quad \boldsymbol{r}_{B1} = \left(1, \frac{1}{2}\right)\,, \quad \boldsymbol{r}_{B2} = \left(\frac{1}{2}, 1\right)\,. \tag{11}$$

For site i, we shall find it helpful to separate out the dimer center $\boldsymbol{d}_i$ with $i = A, B$

$$\boldsymbol{d}_A = \left(\frac{1}{4}, \frac{1}{4}\right)\,, \quad \boldsymbol{d}_B = \left(\frac{3}{4}, \frac{3}{4}\right) \tag{12}$$

and the spin relative to the dimer center $\boldsymbol{s}_i$ where, implicitly, the latter depends on the index A or B of the sublattice

$$\boldsymbol{s}_{A1} = \left(-\frac{1}{4}, -\frac{1}{4}\right)\,, \quad \boldsymbol{s}_{A2} = \left(\frac{1}{4}, \frac{1}{4}\right)\,, \quad \boldsymbol{s}_{B1} = \left(\frac{1}{4}, -\frac{1}{4}\right)\,, \quad \boldsymbol{s}_{B2} = \left(-\frac{1}{4}, +\frac{1}{4}\right)\,. \tag{13}$$

The magnetic interactions consist of nearest-neighbor and next-nearest-neighbor Heisenberg exchange

$$H = J_D \sum_{\langle i,j \rangle} \boldsymbol{S}_i \cdot \boldsymbol{S}_j + J \sum_{\langle\langle i,j \rangle\rangle} \boldsymbol{S}_i \cdot \boldsymbol{S}_j. \tag{14}$$

The ground state of the model for $J/J_D \lesssim 0.65$ is a dimer covering with singlets on sites $A1 - A2$ and $B1 - B2$ which are coupled by J_D. This breaks no symmetries and there is a crossover as the temperature is lowered.

It is convenient to work with a bond wave representation of the ground state and magnetic excitations due to Sachdev and Bhatt [5]. The starting point is to introduce operators that create singlet and triplet states from the vacuum. In the Shastry-Sutherland model these operators are

4

defined on all dimers.

$$|s\rangle = s^\dagger|\text{VAC}\rangle = \frac{1}{\sqrt{2}}\left(|\uparrow\downarrow\rangle - |\downarrow\uparrow\rangle\right),\tag{15a}$$

$$|t_x\rangle = t_x^\dagger|\text{VAC}\rangle = -\frac{1}{\sqrt{2}}\left(|\uparrow\uparrow\rangle - |\downarrow\downarrow\rangle\right),\tag{15b}$$

$$|t_y\rangle = t_y^\dagger|\text{VAC}\rangle = \frac{i}{\sqrt{2}}\left(|\uparrow\uparrow\rangle + |\downarrow\downarrow\rangle\right),\tag{15c}$$

$$|t_z\rangle = t_z^\dagger|\text{VAC}\rangle = \frac{1}{\sqrt{2}}\left(|\uparrow\downarrow\rangle + |\downarrow\uparrow\rangle\right).\tag{15d}$$

These must satisfy the constraint

$$s^\dagger s + \sum_\alpha t_\alpha^\dagger t_\alpha = 1.\tag{16}$$

In terms of the singlet and triplet operators, the spin one-half operators are

$$S_1^\alpha = \frac{1}{2}\left(s^\dagger t_\alpha + t_\alpha^\dagger s - i\epsilon_{\alpha\beta\gamma}t_\beta^\dagger t_\gamma\right),\tag{17a}$$

$$S_2^\alpha = \frac{1}{2}\left(-s^\dagger t_\alpha - t_\alpha^\dagger s - i\epsilon_{\alpha\beta\gamma}t_\beta^\dagger t_\gamma\right).\tag{17b}$$

The intra-dimer exchange coupling $\boldsymbol{S}_1\cdot\boldsymbol{S}_2$ can be written in terms of the bond operators as follows:

$$-\frac{3}{4}s^\dagger s + \frac{1}{4}\sum_{\alpha=x,y,z} t_\alpha^\dagger t_\alpha,\tag{18}$$

after imposing the constraint.

An example of an exchange coupling between neighboring dimers is

$$\frac{1}{2}i\epsilon_{\alpha\beta\gamma}t_{i\beta}^\dagger t_{i\gamma}\left(s_j^\dagger t_{j\alpha} + t_{j\alpha}^\dagger s_j - i\epsilon_{\alpha\sigma\tau}t_{j\sigma}^\dagger t_{j\tau}\right),\tag{19}$$

where the triplon indices are in the Cartesian basis x, y, z.

Taken together Eqs. (18) and (19) reveal that, for sufficiently small J/J_D, the ground state is obtained by condensing singlets while the lowest energy excitations are triply degenerate "triplons" lying at energy J_D. As the coupling between singlets has no quadratic terms at this bare level the triplons are completely localized or, in momentum space, there are flat bands at energy J_D (to leading order in J/J_D).

J/J_D PERTURBATION THEORY AND BOUND STATES

Now we consider the effects of carrying out perturbation theory in J/J_D within the dimer phase. In the material, $SrCu_2(BO_3)_2$, $J/J_D \approx 0.6$ and therefore not obviously in the perturbative regime

in the inter-dimer hopping. It turns out that physics in the Shastry-Sutherland model is remarkably localized especially in the ground state but also within the single triplon sector. In essence this localization, which originates from geometrical frustration of the Heisenberg coupling on this lattice, makes the perturbative treatment meaningful for much larger inter-dimer couplings than one might naively expect. This section essentially reviews results in Refs. [6–10]. We also refer the reader to a review [11] for a broader context.

Single triplon states

As we have seen, the bare Hamiltonian to quadratic order has perfectly localized triplons. The single triplon gap is renormalized downwards by triplon interactions with the leading order contribution appearing already at $O((J/J_D)^2)$. To 4th order in J/J_D one finds:

$$\Delta = J_D \left(1 - \left(\frac{J}{J_D} \right)^2 - \frac{1}{2} \left(\frac{J}{J_D} \right)^3 - \frac{1}{8} \left(\frac{J}{J_D} \right)^4 \right). \tag{20}$$

This is in very good agreement with exact diagonalization results throughout the dimer phase (see Fig. 4 in the main text).

Interaction effects also introduce a dispersion for the triplons. Eq. (19) contains cubic terms in the triplon operators of the schematic form $t_i^\dagger t_i (t_j + t_j^\dagger)$ that effect a creation or annihilation of a triplon in the presence of a neighboring triplon. One can show that this term introduces an effective direct hopping term for the triplons to sixth order in perturbation theory [11–13]. The material $SrCu_2(BO_3)_2$, that is reasonably well described by the Shastry-Sutherland model in the dimer phase, has $J/J_D \approx 0.6$ placing it close to the phase boundary of the dimer phase. For this value of J/J_D the single triplon dispersion is around 5% of the triplon gap so the bands remain quite flat [12]. Fig. 1 shows data from 28 site exact diagonalization recording the single triplon bandwidth as a function of J/J_D. The sixth order leading contribution to the bandwidth is evident from the figure with departures evident at larger coupling.

An important contribution to the triplon dispersion in the material comes from a Dzyaloshinsky-Moriya interaction (DMI). The magnitude of the DMI is roughly 5% of J_D [11, 14] and a direct fit of experimental data has been performed in Ref. [15]. The effects of DMI are particularly evident as they break the degeneracy of the triplon modes. As we shall see, the bound state modes in a given sector disperse on the scale of J^2 but there is a splitting between sectors on the scale of J. Therefore the overall bandwidth of low-lying triplon states is dominated by the bound states
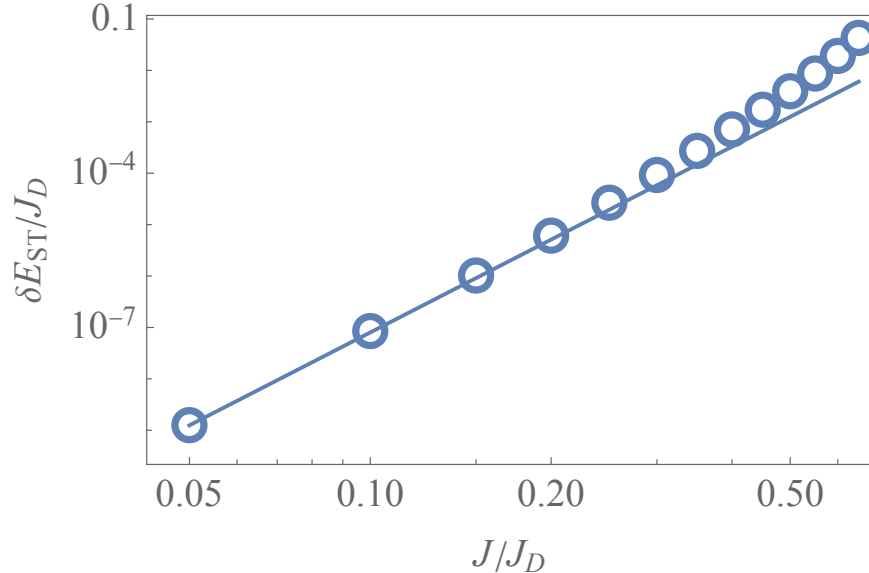
FIG. 1. Difference between maximum and minimum single triplon energies from $N = 28$ exact diagonalization as a function of J/J_D and on a log-log scale (open circles). The straight line passing through the small J/J_D points is $\delta E_{ST} \sim (J/J_D)^6$.

and not by the presence of DMI. So while DMI certainly contributes to thermal broadening of the modes in the material (see also Section), the principal effect is captured already in the pure Shastry-Sutherland model. Therefore we neglect the effects coming from DMI in the material.

Two triplon states

As remarked on above, the exact dispersion relation of the single triplon states has a bandwidth that is much smaller than the triplon gap. This directly implies that the two triplon continuum is very narrow. Overall, geometrical frustration makes itself felt through the exact dimer ground state and through the presence of nearly localized triplon modes. The first place where the bare interactions generate physics almost on the scale of those interactions is through bound states of two triplons. It turns out that these are split on the scale of J and disperse on the scale of J^2.

To third order in J/J_D the bound and anti-bound states are composed of eight distinct triplon configurations up to lattice translations [10, 11]. These are shown in Fig. 2. For example, the states labeled (a) and (b) in sector I are connected by two correlated hopping processes generated from the cubic terms in perturbation theory where one process creates a triplon on the left which then annihilates a triplon at the top. The configurations shown participate for each of the bound
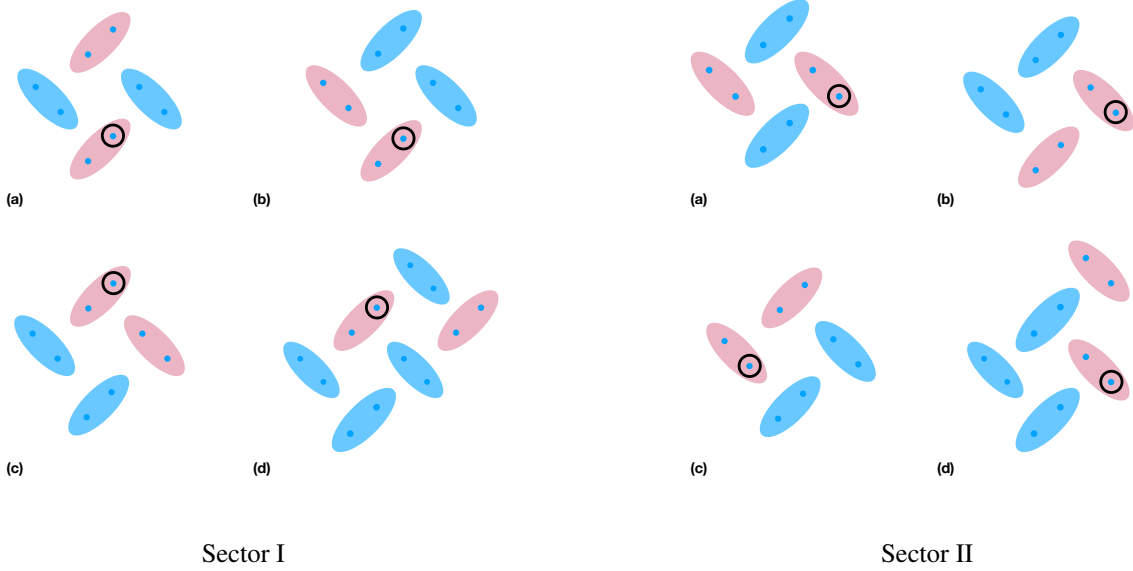
FIG. 2. Two triplon bound states connected to order $(J'/J)^3$. Sectors I and II are distinct at least up to third order.

state angular momentum sectors $S = 0, 1, 2$. The two sectors I and II are not connected to third order in perturbation theory. They are connected at higher order where also more configurations must be included.

The general form of an effective tight-binding model for Sector I is

$$H_I(\boldsymbol{q}) = \begin{pmatrix} 2\Delta + V_{\mathrm{NNN}} & J_{\mathrm{NN}} & J_{\mathrm{NN}}e^{iq_y} & 0 \\ J_{\mathrm{NN}} & 2\Delta + V_{\mathrm{NN}} & J_3 & -J_{\mathrm{NN}}e^{iq_x} \\ J_{\mathrm{NN}}e^{-iq_y} & J_3 & 2\Delta + V_{\mathrm{NN}} & -J_{\mathrm{NN}} \\ 0 & -J_{\mathrm{NN}}e^{-iq_x} & -J_{\mathrm{NN}} & 2\Delta + V_{\mathrm{NNN}} \end{pmatrix} \tag{21}$$

where aside from the gap Δ in Eq. (20), the entries in the matrix depend on S. In particular, one finds for $S = 2$:

$$V_{\mathrm{NN}} = \frac{J}{2} + \frac{J^2}{2J_D} - \frac{J^3}{8J_D{}^2} \tag{22}$$

$$V_{\mathrm{NNN}} = \frac{J^3}{4J_D{}^2} \tag{23}$$

$$J_{\mathrm{NN}} = \frac{J^2}{4J_D} + \frac{5J^3}{16J_D{}^2} \tag{24}$$

$$J_3 = \frac{J^2}{4J_D} + \frac{3J^3}{8J_D{}^2} \tag{25}$$

8

for $S = 1$:

$$V_{\text{NN}} = -\frac{J}{2} + \frac{J^2}{J_D} + \frac{7J^3}{8J_D{}^2} \tag{26}$$

$$V_{\text{NNN}} = -\frac{J^3}{4J_D{}^2} \tag{27}$$

$$J_{\text{NN}} = -\frac{J^2}{4J_D} - \frac{3J^3}{16J_D{}^2} \tag{28}$$

$$J_3 = \frac{J^2}{4J_D} + \frac{J^3}{8J_D{}^2} \tag{29}$$

and for $S = 0$:

$$V_{\text{NN}} = -J + \frac{J^2}{2J_D} + \frac{J^3}{J_D{}^2} \tag{30}$$

$$V_{\text{NNN}} = -\frac{J^3}{2J_D{}^2} \tag{31}$$

$$J_{\text{NN}} = -\frac{J^2}{2J_D} - \frac{J^3}{4J_D{}^2} \tag{32}$$

$$J_3 = -\frac{J^2}{2J_D}. \tag{33}$$

These results reveal that components (b) and (c) are bound to leading order in J with splitting $+J/2$, $-J/2$ and $-J$ respectively for $S = 2, 1, 0$. Dispersion appears to order J^2. Sector II Hamiltonians are obtained by taking $A \leftrightarrow B$ and $q_x \to q_y$ and $q_y \to -q_x$.

The basis states for the bound states within each angular momentum sector take the form:

$$|\Phi_{0,0}\rangle = \Phi_{0,0}^\dagger |0\rangle = \frac{1}{\sqrt{3}} \left(t_1^\dagger t_{-1}^\dagger - t_0^\dagger t_0^\dagger + t_{-1}^\dagger t_1^\dagger \right) |0\rangle \tag{34}$$

$$|\Phi_{1,0}\rangle = \Phi_{1,0}^\dagger |0\rangle = \frac{1}{\sqrt{2}} \left(t_1^\dagger t_{-1}^\dagger - t_{-1}^\dagger t_1^\dagger \right) |0\rangle \tag{35}$$

$$|\Phi_{2,0}\rangle = \Phi_{2,0}^\dagger |0\rangle = \frac{1}{\sqrt{6}} \left(t_1^\dagger t_{-1}^\dagger + 2t_0^\dagger t_0^\dagger + t_{-1}^\dagger t_1^\dagger \right) |0\rangle \tag{36}$$

$$|\Phi_{1,1}\rangle = \Phi_{1,1}^\dagger |0\rangle = \frac{1}{\sqrt{2}} \left(t_1^\dagger t_0^\dagger - t_0^\dagger t_1^\dagger \right) |0\rangle \tag{37}$$

$$|\Phi_{1,-1}\rangle = \Phi_{1,-1}^\dagger |0\rangle = \frac{1}{\sqrt{2}} \left(t_0^\dagger t_{-1}^\dagger - t_{-1}^\dagger t_0^\dagger \right) |0\rangle \tag{38}$$

$$|\Phi_{2,1}\rangle = \Phi_{2,1}^\dagger |0\rangle = \frac{1}{\sqrt{2}} \left(t_1^\dagger t_0^\dagger + t_0^\dagger t_1^\dagger \right) |0\rangle \tag{39}$$

$$|\Phi_{2,-1}\rangle = \Phi_{2,-1}^\dagger |0\rangle = \frac{1}{\sqrt{2}} \left(t_0^\dagger t_{-1}^\dagger + t_{-1}^\dagger t_0^\dagger \right) |0\rangle \tag{40}$$

$$|\Phi_{2,2}\rangle = \Phi_{2,2}^\dagger |0\rangle = t_1^\dagger t_1^\dagger |0\rangle \tag{41}$$

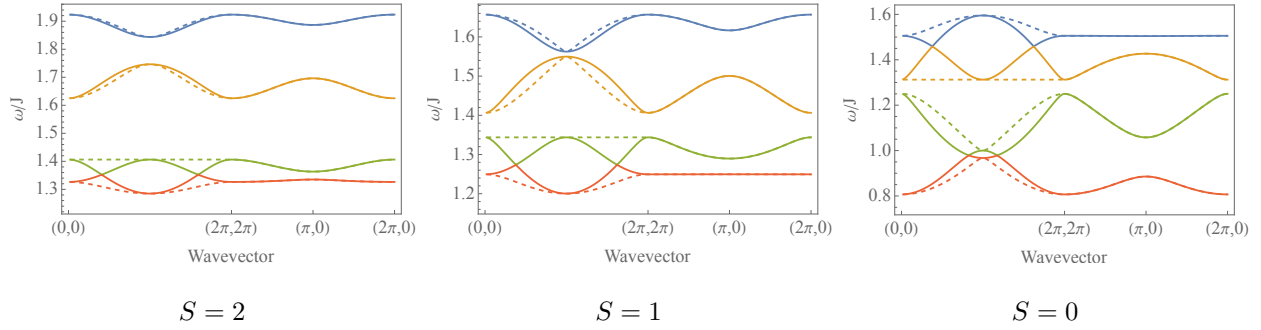$$|\Phi_{2,-2}\rangle = \Phi_{2,-2}^\dagger |0\rangle = t_{-1}^\dagger t_{-1}^\dagger |0\rangle. \tag{42}$$

FIG. 3. Spectra of bound states to third order in perturbation theory in $J/J_D = 0.5$. From left to right these are for $S = 2$, $S = 1$ and $S = 0$ angular momentum sectors. Solid lines are for Sector I and dashed lines for Sector II.

Using the configuration labels in real space in Fig. 2 we specify a notation for the two-triplon bound states. We label these configurations by $\mu = a, b, c, d$ for the configuration and $\sigma = I, II$ for the sector and refer each to the highlighted primitive cell position. We also need a label S, m for the angular momentum sector. In momentum space the states are

$$|\boldsymbol{P}, \mu, \sigma; S, m\rangle \equiv \frac{1}{\sqrt{N}} \sum_i \exp\left(i\boldsymbol{P} \cdot \boldsymbol{R_i}\right)|\boldsymbol{R_i}, \mu, \sigma; S, m\rangle. \qquad (43)$$

The eigenstates are denoted $|\boldsymbol{P}, M, \sigma; S, m\rangle$ where M runs over the four bands in each of the two sectors.

The two-triplon bound states, $|\boldsymbol{P}, M, \sigma; S, m\rangle$ for eigenvalue M, obtained by diagonalizing the Hamiltonians given above, are

$$|\boldsymbol{P}, M, \sigma; S, m\rangle = \sum_{\mu=1}^{4} v_\mu^M(\boldsymbol{P}, S, \sigma)|\boldsymbol{P}, \mu, \sigma; S, m\rangle. \qquad (44)$$

The spectra of the two-triplon bound states to third order in perturbation theory in J/J_D are shown in Fig. 3. Each panel is for a different total angular momentum sector $S = 2, 1, 0$ and each panel contains eight modes $-$ four for each of sectors I and II defined above. Fig. 4 in the main text illustrates that the perturbative bound state band widths are in reasonable agreement with exact diagonalization results for J/J_D even as large as ~ 0.5. One notices from these figures that the lowest energy bound state mode lives in the singlet sector and that this crosses the single triplon energy at about $J/J_D = 0.539$ (perturbation theory) and roughly $J/J_D = 0.585$ (28 site ED). In SrCu$_2$(BO$_3$)$_2$, the exchange parameters are such that the lowest energy bound state mode is at about the single triplon energy.

$\Gamma_{d'\sigma\mu}$	d'	
	A	B
Ia	$e^{i\boldsymbol{q}\cdot\hat{\boldsymbol{y}}} + e^{i(\boldsymbol{p}-\boldsymbol{q})\cdot\hat{\boldsymbol{y}}}$	0
Ib	$e^{-i(\boldsymbol{p}-\boldsymbol{q})\cdot\hat{\boldsymbol{x}}}$	$e^{-i\boldsymbol{q}\cdot\hat{\boldsymbol{x}}}$
Ic	$e^{-i(\boldsymbol{p}-\boldsymbol{q})\cdot\hat{\boldsymbol{y}}}$	$e^{-i\boldsymbol{q}\cdot\hat{\boldsymbol{y}}}$
Id	$e^{i\boldsymbol{q}\cdot\hat{\boldsymbol{x}}} + e^{i(\boldsymbol{p}-\boldsymbol{q})\cdot\hat{\boldsymbol{x}}}$	0
IIa	0	$e^{-i\boldsymbol{q}\cdot\hat{\boldsymbol{x}}} + e^{-i(\boldsymbol{p}-\boldsymbol{q})\cdot\hat{\boldsymbol{x}}}$
IIb	1	1
IIc	$e^{i\boldsymbol{q}\cdot(\hat{\boldsymbol{x}}+\hat{\boldsymbol{y}})}$	$e^{i(\boldsymbol{p}-\boldsymbol{q})\cdot(\hat{\boldsymbol{x}}+\hat{\boldsymbol{y}})}$
IId	0	$e^{i\boldsymbol{q}\cdot\hat{\boldsymbol{y}}} + e^{i(\boldsymbol{p}-\boldsymbol{q})\cdot\hat{\boldsymbol{y}}}$

TABLE I. Matrix element contribution $\Gamma_{d\sigma\mu}(\boldsymbol{p} - \boldsymbol{q}, \boldsymbol{q})$ defined in Eq. (46).

For the susceptibility contribution we require single triplon to bound state matrix elements:

$$\langle \boldsymbol{p}, \mu, \sigma; S, m | S^z_{\boldsymbol{i}ds} | \boldsymbol{q}, d', \tilde{m} \rangle \tag{45}$$

and we use the notation

$$\langle \boldsymbol{p}, \mu, \sigma; S, m | S^z_{\boldsymbol{i}ds} | \boldsymbol{q}, d', \tilde{m} \rangle \equiv \delta(d, d'; \sigma, \mu)\delta_{m,\tilde{m}}(1/N)(-)^{s+1}\alpha^{S,m}_{\tilde{m}} e^{-i(\boldsymbol{p}-\boldsymbol{q})\cdot\boldsymbol{R}_i}\Gamma_{d'\sigma\mu}(\boldsymbol{p} - \boldsymbol{q}, \boldsymbol{q}) \tag{46}$$

where $\delta(d, d'; \sigma, \mu)$ enforces the constraints listed below on the dimer sublattices for a given configuration μ. The $\Gamma_{dd'\sigma\mu}(\boldsymbol{p} - \boldsymbol{q}, \boldsymbol{q})$ and $\delta(d, d'; \sigma, \mu)$ are listed in the tables I and II, respectively.

The coefficients $\alpha^{S,m}_{\tilde{m}}$ place constraints on the sum over the spin sectors and the resulting angular momentum degeneracies. In the susceptibilities they appear squared thus:

$$\left(\alpha^{0,0}_0\right)^2 = \frac{1}{12} \tag{47}$$

$$\left(\alpha^{2,0}_0\right)^2 = \frac{1}{6} \tag{48}$$

$$\left(\alpha^{1,1}_1\right)^2 = \frac{1}{8} \tag{49}$$

$$\left(\alpha^{1,-1}_{-1}\right)^2 = \frac{1}{8} \tag{50}$$

$$\left(\alpha^{2,1}_1\right)^2 = \frac{1}{8} \tag{51}$$

$$\left(\alpha^{2,-1}_{-1}\right)^2 = \frac{1}{8}. \tag{52}$$

Evidently $\tilde{m} = m$ because S^z preserves a $U(1)$ while breaking overall spin rotation symmetry.

11

$\delta(d, d'; \sigma, \mu)$	d'	
	A	B
Ia	δ_{dA}	—
Ib	δ_{dB}	δ_{dA}
Ic	δ_{dB}	δ_{dA}
Id	δ_{dA}	—
IIa	—	δ_{dB}
IIb	δ_{dB}	δ_{dA}
IIc	δ_{dB}	δ_{dA}
IId	—	δ_{dB}

TABLE II. Matrix element contribution $\delta(d, d'; \sigma, \mu)$ defined in Eq. (46).

SUSCEPTIBILITY CONTRIBUTIONS

The contribution to the susceptibility arising from transitions from the ground state to the single triplon states is

$$\chi^{zz}(\boldsymbol{q}, \omega)|_{01/10;AA} = \frac{1}{Z}\frac{1}{8}(1 - e^{-\beta\Delta}) \left[1 - \cos\left(\frac{q_x + q_y}{2}\right)\right] \left(\frac{1}{\omega + i\eta - \Delta} - \frac{1}{\omega + i\eta + \Delta}\right) \quad (53)$$

$$\chi^{zz}(\boldsymbol{q}, \omega)|_{01/10;BB} = \frac{1}{Z}\frac{1}{8}(1 - e^{-\beta\Delta}) \left[1 - \cos\left(\frac{q_x - q_y}{2}\right)\right] \left(\frac{1}{\omega + i\eta - \Delta} - \frac{1}{\omega + i\eta + \Delta}\right) \quad (54)$$

for the A and B sublattice dimers. For convenience, we show again the form of the single particle propagator (Eq. (7)) that follows from these equations

$$D(\boldsymbol{q}, \omega) = \frac{1}{8} \left[2 - \cos\left(\frac{q_x + q_y}{2}\right) - \cos\left(\frac{q_x - q_y}{2}\right)\right] \left(\frac{1}{\omega + i\eta - \Delta} - \frac{1}{\omega + i\eta + \Delta}\right). \quad (55)$$

Here we have assumed that the triplons are dispersionless with energy Δ (Eq. (20)). The dynamical structure factor computed from this susceptibility is delta peaked at the single triplon energy and only the coefficient of the delta function is temperature dependent. We note that only matrix elements connecting the ground state to the $S^z = 0$ single triplon states contribute to the susceptibility.

For perfectly localized triplon modes, the matrix elements connecting single triplon to single triplon states vanish so that the contribution C_{11} in Eq. (10) for the self-energy is zero. As we have discussed, this ceases to be the case once high order perturbative processes are included that allow

for single triplon hopping. This can be expected to give the leading contribution to the direct broadening of the delta function peak at the single triplon energies. However, the resulting linewidth is bounded by the very narrow bandwidth of the triplon mode and therefore cannot account for the extent of the observed broad response in energy. In the following we work consistently with the flat triplon mode.

We now report the part of the susceptibility connecting the single triplon states with unbound two triplon states first of all without any restriction on the number of the latter states coming from the presence of bound states.

$$\chi^{zz}(\boldsymbol{q},\omega)|_{12(\text{free});AA} = \frac{1}{8Z}\frac{3}{4}(4N+2)\left(\frac{e^{-\beta\Delta} - e^{-2\beta\Delta}}{\omega + i\eta - \Delta}\right)\left[1 - \cos\left(\frac{q_x + q_y}{2}\right)\right] \qquad (56)$$

$$\chi^{zz}(\boldsymbol{q},\omega)|_{12(\text{free});BB} = \frac{1}{8Z}\frac{3}{4}(4N+2)\left(\frac{e^{-\beta\Delta} - e^{-2\beta\Delta}}{\omega + i\eta - \Delta}\right)\left[1 - \cos\left(\frac{q_x - q_y}{2}\right)\right]. \qquad (57)$$

We note that the pieces proportional to N are identical to the ground state to single triplon contribution to the susceptibility after multiplying by $3Ne^{-\beta\Delta}D(\boldsymbol{q},\omega)$ which is nothing other than $(1 - e^{-\beta\Delta})Z_1 D(\boldsymbol{q},\omega)$ in Eq. (10) where Z_1 is the single triplon contribution to the partition sum.

The susceptibility connecting single triplon to two free triplon states given above overcounts because some of the two free triplon states participate in bound states. In particular, inspection of the matrix element connecting single triplons to two free triplon states reveals that for fixed initial and final state momentum and with one primitive lattice position fixed by the spin whose matrix element is computed, there remains a sum over real space positions. Within this sum there are contributions coming from configurations illustrated in Fig. 2. In other words, the matrix element is corrected from $M(\boldsymbol{p}_1, \boldsymbol{p}_2, \boldsymbol{p}, \boldsymbol{i})$ to $M(\boldsymbol{p}_1, \boldsymbol{p}_2, \boldsymbol{p}, \boldsymbol{i}) - \delta M$ where the δM subtracts off the configurations that contribute to the bound states. Once these have been accounted for we find for the free triplon contribution

$$(C_{12} + C_{21})|_{\text{free}} - (1 - e^{-\beta\Delta})Z_1 D(\boldsymbol{q},\omega)$$
$$= -\frac{21}{16}\left(e^{-\beta\Delta} - e^{-2\beta\Delta}\right)F(q_x, q_y)\left(\frac{1}{\omega + i\eta - \Delta} - \frac{1}{\omega + i\eta + \Delta}\right) \qquad (58)$$

where

$$F(q_x, q_y) = \left[2 - \cos\left(\frac{q_x + q_y}{2}\right) - \cos\left(\frac{q_x - q_y}{2}\right)\right]. \qquad (59)$$

Here we have accounted for the factor 2 coming from the sum over spins for a fixed dimer. This has $1/\eta^2$ divergences like the single triplon propagator. Evidently, this term contributes only at the single triplon energy and is suppressed exponentially in the single triplon gap.

By considering the bound states of two triplons we find a response over a broad energy range. The contributions to Eq. (10) are

$$
C_{12}|_{\text{bound}} = \frac{1}{4N} \sum_{\boldsymbol{k},m,d,\sigma,\mu,\tilde{\mu}} \sum_{d_i,d_j,s_i,s_j} e^{-i\boldsymbol{q}\cdot(\boldsymbol{d}_i-\boldsymbol{d}_j+\boldsymbol{s}_i-\boldsymbol{s}_j)} \left(\alpha_m^{S,m}\right)^2 (-)^{s_i+s_j} \delta(d_i,d;\sigma,\mu)\delta(d_j,d;\sigma,\tilde{\mu})
$$

$$
\Gamma_{d\sigma\tilde{\mu}}(\boldsymbol{q},\boldsymbol{k}-\boldsymbol{q})\Gamma_{d\sigma\mu}^*(\boldsymbol{q},\boldsymbol{k}-\boldsymbol{q}) \left(\frac{e^{-\beta\Delta}-e^{-\beta E_{\boldsymbol{k},M,S,\sigma}^{(2)}}}{\omega+i\eta+\Delta-E_{\boldsymbol{k},M,S,\sigma}^{(2)}}\right) v_\mu^M(\boldsymbol{k},S,\sigma)v_{\tilde{\mu}}^{*M}(\boldsymbol{k},S,\sigma)
$$

(60)

and

$$
C_{21}|_{\text{bound}} = \frac{1}{4N} \sum_{\boldsymbol{k},m,d,\sigma,\mu,\tilde{\mu}} \sum_{s_i,s_j} e^{-i\boldsymbol{q}\cdot(\boldsymbol{d}_i-\boldsymbol{d}_j+\boldsymbol{s}_i-\boldsymbol{s}_j)} \left(\alpha_m^{S,m}\right)^2 (-)^{s_i+s_j} \delta(d_i,d;\sigma,\mu)\delta(d_j,d;\sigma,\tilde{\mu})
$$

$$
\Gamma_{d\sigma\mu}(-\boldsymbol{q},\boldsymbol{k}+\boldsymbol{q})\Gamma_{d\sigma\tilde{\mu}}^*(-\boldsymbol{q},\boldsymbol{k}+\boldsymbol{q}) \left(\frac{e^{-\beta E_{\boldsymbol{k},M,S,\sigma}^{(2)}}-e^{-\beta\Delta}}{\omega+i\eta+E_{\boldsymbol{k},M,S,\sigma}^{(2)}-\Delta}\right) v_\mu^{*M}(\boldsymbol{k},S,\sigma)v_{\tilde{\mu}}^M(\boldsymbol{k},S,\sigma).
$$

(61)

As noted above, in $SrCu_2(BO_3)_2$ the minimum energy singlet two-triplon bound states coincide with the single triplon energy. Eq. (60) implies, then, that there is an inelastic response in the Shastry-Sutherland model at finite temperatures extending from very low energies. In particular, the lowest energy bound states live in the singlet sector $S = 0$ for which the energies $E_{\boldsymbol{k},M,0,\sigma}^{(2)}$ extend upwards from around Δ. Therefore the condition $\omega = E_{\boldsymbol{k},M,S,\sigma}^{(2)} - \Delta$ (from the denominator in Eq. (60)) "clicks" at energies ω much smaller than Δ. This is the central observation accounting for the experimentally observed broad response in the material.

In the main text we present results from a direct evaluation of the dynamical structure factor (Eqs. (1) and (9)) including the expression Eq. (10) for the self-energy. The integration over momenta in the bound state contribution to C_{12} and C_{21} is performed numerically with fixed finite η. The number of integration points N is chosen to reach convergence with integration grid fine enough to be significantly smaller than the artificial width set by η. The width η itself is chosen to be $0.004J_D$ so much smaller than the bandwidth of the bound states.

The results reveal a very broad temperature dependent inelastic response originating from the bound state modes that are low-lying in relation to the single triplon modes. The single triplon peak remains delta spiked in our calculation unlike the triplon mode in the alternating Heisenberg chain studied by James et $al.$ [2]. The origin of the difference is the presence of $1/\eta^4$ divergences at the single triplon energy in the one-to-two particle susceptibility in the one dimensional case that are

14

cured by computing the resummed self-energy. In the Shastry-Sutherland model, the divergences are much less severe. There are logarithmic divergences in the one-to-two particle susceptibility in the Shastry-Sutherland model in the bound state channel coming from van Hove singularities in the bound state band structure at various energies depending on J/J_D that are presumably resolved at higher order in the low temperature expansion. There is also a $1/\eta^2$ divergence coming from one to two free triplon susceptibility that have the effect of reducing the spectral weight in the delta peak as a function of temperature.

Finally, we remark on the connection between the Shastry-Sutherland model and thermal broadening in other quantum magnets. As shown in the main text the magnitude and temperature dependence of the thermal broadening in $SrCu_2(BO_3)_2$ are captured by dynamical METTS on the Shastry-Sutherland model. The low temperature expansion suggests that the origin of this anomalous broadening is the small gap between the single triplon modes and the bound states. An intuition for this effect is that when there is a small thermal population of triplons at low temperature, excitation of a second triplon spectroscopically can have weight in the singlet bound state sector at very low energies thus producing a broad response. The magnitude of this response is expected to increase with the ambient thermal population of triplons.

What sets the Shastry-Sutherland model apart from typical quantum magnets in this regard? The answer would seem to rely on the peculiar fine-tuning of $SrCu_2(BO_3)_2$. Other quantum magnets, for the purposes of this discussion, typically fall into two classes: gapped and (nearly) gapless. Gapless quantum magnets have single particle modes appearing, for the most part, among two particle states in the same energy range with broadening induced at zero temperature by matrix elements connecting these states. We would typically not expect thermal broadening to be especially dramatic in such gapless systems as there is (i) a broad continuum at low energies and (ii) zero temperature broadening. If, instead, the magnet is gapped on scale Δ, it is typical for the two particle states to have minimum at 2Δ. This means that the thermal response is expected at $\omega \sim \Delta$. In contrast, in $SrCu_2(BO_3)_2$, it begins at low energies because the material is poised close to a phase boundary connected to the condensation of bound states so that states are available at anomalously low energies compared to the single particle gap.

FURTHER REMARKS ON SINGLE TRIPLON BROADENING

In the previous section, we pointed out that, when working consistently to third order in J/J_D perturbation theory, the triplon modes are dispersionless and that the susceptibility coming from one triplon to one triplon processes, C_{11}, vanishes. The triplons in the Shastry-Sutherland model, however, do disperse albeit weakly. The, leading order, contribution to the hopping (at sixth order in J/J_D) is between identical neighboring sublattices so the single triplon Hamiltonian remains diagonal in this basis. Even higher order processes break the six-fold degenerate triplons into a pair of three-fold degenerate modes. DMI is known to be an important component of the magnetic couplings in $SrCu_2(BO_3)_2$ at roughly the 10% level and it leads directly to a hopping term for the triplons.

Here we compute the susceptibility C_{11} in the presence of triplon dispersion and estimate the importance of this contribution to the finite temperature response compared to the contributions coming from bound states of two triplons. In general the relevant contribution to the susceptibility is

$$\chi^{zz}(\boldsymbol{q}, \omega) = \frac{1}{4NZ} \sum_{m,m',d,d'} \sum_{\boldsymbol{p},\boldsymbol{k},\boldsymbol{I},\boldsymbol{J}} e^{-i\boldsymbol{q}\cdot(\boldsymbol{I}-\boldsymbol{J})} \langle \boldsymbol{p}dm|S_{\boldsymbol{I}}^z|\boldsymbol{k}d'm'\rangle \langle \boldsymbol{k}d'm'|S_{\boldsymbol{J}}^z|\boldsymbol{p}dm\rangle \left(\frac{e^{-\beta E_{\boldsymbol{p}}} - e^{-\beta E_{\boldsymbol{k}}}}{\omega + i\eta + E_{\boldsymbol{p}} - E_{\boldsymbol{k}}} \right)$$

(62)

where $E_{\boldsymbol{p}}$ is the single triplon energy at momentum $\boldsymbol{p}$.

If the hopping matrix element is diagonal in the sublattice basis then we obtain

$$C_{11}(\boldsymbol{q}, \omega) = \frac{1}{2N} \sum_{\boldsymbol{k}} \left(1 + \cos\left(\frac{q_x}{2}\right) \cos\left(\frac{q_y}{2}\right) \right) \left(\frac{e^{-\beta E_{\boldsymbol{k}-\boldsymbol{q}}} - e^{-\beta E_{\boldsymbol{k}}}}{\omega + i\eta + E_{\boldsymbol{k}-\boldsymbol{q}} - E_{\boldsymbol{k}}} \right).$$

(63)

Evidently, if the triplon bandwidth goes to zero, this contribution vanishes as previously claimed.

The details of the C_{11} contribution to the dynamical response function depends on the nature of the dispersion relation and the magnetic couplings. However, Eq. (63) can be expected to capture the general dependence on energy ω. For single triplon modes with bandwidth $2g \ll \Delta$, C_{11} will have its principal effect at low energies extending up to $\omega = 4g$. To put this in perspective the bandwidth in $SrCu_2(BO_3)_2$ is about 10% of the 3 meV gap so one should expect the single triplon dispersion to contribute up to an energy of about 0.6 meV independent of the nature of the matrix elements. DMI will tend to introduce some small direct broadening of the single triplon peak but this is expected to be much smaller than the broad contribution originating from the bound states as the imaginary part of the self-energy is suppressed at higher energies than $4g$.

[1] F. H. L. Essler and R. M. Konik, Finite-temperature lineshapes in gapped quantum spin chains, Phys. Rev. B **78**, 100403 (2008).

[2] A. J. A. James, F. H. L. Essler, and R. M. Konik, Finite-temperature dynamical structure factor of alternating Heisenberg chains, Phys. Rev. B **78**, 094411 (2008).

[3] E. S. Klyushina, A. C. Tiegel, B. Fauseweh, A. T. M. N. Islam, J. T. Park, B. Klemke, A. Honecker, G. S. Uhrig, S. R. Manmana, and B. Lake, Magnetic excitations in the $S = \frac{1}{2}$ antiferromagnetic-ferromagnetic chain compound $BaCu_2V_2O_8$ at zero and finite temperature, Phys. Rev. B **93**, 241109 (2016).

[4] B. Fauseweh, F. Groitl, T. Keller, K. Rolfs, D. A. Tennant, K. Habicht, and G. S. Uhrig, Time-dependent correlations in quantum magnets at finite temperature, Phys. Rev. B **94**, 180404 (2016).

[5] S. Sachdev and R. N. Bhatt, Bond-operator representation of quantum spins: Mean-field theory of frustrated quantum Heisenberg antiferromagnets, Phys. Rev. B **41**, 9323 (1990).

[6] P. Lemmens, M. Grove, M. Fischer, G. Güntherodt, V. N. Kotov, H. Kageyama, K. Onizuka, and Y. Ueda, Collective Singlet Excitations and Evolution of Raman Spectral Weights in the 2D Spin Dimer Compound $SrCu_2(BO_3)_2$, Phys. Rev. Lett. **85**, 2605 (2000).

[7] S. Miyahara and K. Ueda, Exact Dimer Ground State of the Two Dimensional Heisenberg Spin System $SrCu_2(BO_3)_2$, Phys. Rev. Lett. **82**, 3701 (1999).

[8] K. Totsuka, S. Miyahara, and K. Ueda, Low-Lying Magnetic Excitation of the Shastry-Sutherland Model, Phys. Rev. Lett. **86**, 520 (2001).

[9] T. Momoi and K. Totsuka, Magnetization plateaus as insulator-superfluid transitions in quantum spin systems, Phys. Rev. B **61**, 3231 (2000).

[10] T. Momoi and K. Totsuka, Magnetization plateaus of the Shastry-Sutherland model for $SrCu_2(BO_3)_2$: Spin-density wave, supersolid, and bound states, Phys. Rev. B **62**, 15067 (2000).

[11] S. Miyahara and K. Ueda, Theory of the orthogonal dimer Heisenberg spin model for $SrCu_2(BO_3)_2$, J. Phys.: Condens. Matter **15**, R327 (2003).

[12] Z. Weihong, C. J. Hamer, and J. Oitmaa, Series expansions for a Heisenberg antiferromagnetic model for $SrCu_2(BO)_3)_2$, Phys. Rev. B **60**, 6608 (1999).

[13] C. Knetter, A. Bühler, E. Müller-Hartmann, and G. S. Uhrig, Dispersion and Symmetry of Bound States in the Shastry-Sutherland Model, Phys. Rev. Lett. **85**, 3958 (2000).

[14] O. Cépas, K. Kakurai, L. P. Regnault, T. Ziman, J. P. Boucher, N. Aso, M. Nishi, H. Kageyama, and Y. Ueda, Dzyaloshinski-Moriya Interaction in the 2D Spin Gap System $SrCu_2(BO_3)_2$, Phys. Rev. Lett. **87**, 167205 (2001).

[15] P. A. McClarty, F. Krüger, T. Guidi, S. F. Parker, K. Refson, A. W. Parker, D. Prabhakaran, and R. Coldea, Topological triplon modes and bound states in a Shastry–Sutherland magnet, Nat. Phys. **13**, 736 (2017).